catalysts

MDPI

Article

Insights into the Structural Dynamics of Pt/CeO_2 Single-Site Catalysts during CO Oxidation

Paolo Dolcet [1], Florian Maurer [1], Maria Casapu [1] and Jan-Dierk Grunwaldt [1,2,*]

[1] Institute for Chemical Technology and Polymer Chemistry (ITCP), Karlsruhe Institute of Technology (KIT), Engesserstraße 20, 76131 Karlsruhe, Germany; paolo.dolcet@kit.edu (P.D.); florian.maurer@kit.edu (F.M.); maria.casapu@kit.edu (M.C.)

[2] Institute of Catalysis Research and Technology (IKFT), Karlsruhe Institute of Technology (KIT), Hermann-von-Helmholtz-Platz 1, 76344 Eggenstein-Leopoldshafen, Germany

* Correspondence: grunwaldt@kit.edu

Abstract: Despite their high atomic dispersion, single site catalysts with Pt supported on CeO_2 were found to have a low activity during oxidation reactions. In this study, we report the behavior of Pt/CeO_2 single site catalyst under more complex gas mixtures, including CO, C_3H_6 and CO/C_3H_6 oxidation in the absence or presence of water. Our systematic *operando* high-energy resolution-fluorescence-detected X-ray absorption near-edge structure (HERFD-XANES) spectroscopic study combined with multivariate curve resolution with alternating least squares (MCR-ALS) analysis identified five distinct states in the Pt single site structure during CO oxidation light-off. After desorption of oxygen and autoreduction of Pt^{4+} to Pt^{2+} due to the increase of temperature, CO adsorbs and reduces Pt^{2+} to $Pt^{\delta+}$ and assists its migration with final formation of $Pt_x^{\Delta+}$ clusters. The derived structure–activity relationships indicate that partial reduction of Pt single sites is not sufficient to initiate the conversion of CO. The reaction proceeds only after the regrouping of several noble metal atoms in small clusters, as these entities are probably able to influence the mobility of the oxygen at the interface with ceria.

Keywords: Pt single sites; *operando*; CO oxidation; X-ray absorption spectroscopy; MCR-ALS

check for updates

Citation: Dolcet, P.; Maurer, F.; Casapu, M.; Grunwaldt, J.-D. Insights into the Structural Dynamics of Pt/CeO_2 Single-Site Catalysts during CO Oxidation. *Catalysts* **2021**, *11*, 617. https://doi.org/10.3390/catal11050617

Academic Editor: Agustín Bueno López

Received: 11 April 2021
Accepted: 7 May 2021
Published: 11 May 2021

Publisher's Note: MDPI stays neutral with regard to jurisdictional claims in published maps and institutional affiliations.

Copyright: © 2021 by the authors. Licensee MDPI, Basel, Switzerland. This article is an open access article distributed under the terms and conditions of the Creative Commons Attribution (CC BY) license (https://creativecommons.org/licenses/by/4.0/).

1. Introduction

In recent years, single atom catalysts (SACs) have attracted increased interest. Especially when noble metals are the active components, an atomically dispersed catalyst would maximize their efficient use. Such systems were found to lead to a high selectivity for hydrogenation and oxidation reactions [1,2]. For Pt/CeO_2-based catalysts, the noble metal single sites are formed either by redispersion of Pt particles under oxidizing conditions at high temperatures (>500 °C) [3] or by trapping of volatile Pt species on the CeO_2 support, as demonstrated by Jones et al. [4]. Despite a perfect active site dispersion, their catalytic activity is not always optimal and, hence, controversially discussed [5–7]. Due to the charge transfer from or to the support and the capacity for adsorption of several ligands, the supported Pt single atoms have been claimed to be resistant to CO poisoning, which is known to affect Pt nanoparticles during CO oxidation [8]. Several groups reported that highly dispersed noble metals form $Ce_{1-X}M_XO_{2-Y}$ species (with M = Pt or Pd), leading to an increase of the catalytic activity in the low temperature regime [9,10]. Additionally, it has been observed that the CO conversion rate increases by treating the SAC with steam at high temperature [10]. This treatment was shown to lead to the formation of $Ce_{1-X}PtO_{2-X}$H–OH species, apparently more active than $Ce_{1-X}PtO_{2-Y}$. However, these findings are in contrast with most of the recent literature reports [4,5,11]. For instance, Gänzler et al. demonstrated that a careful reductive treatment leads to the formation of small Pt nanoparticles and significantly improves the low-temperature oxidation activity of highly dispersed Pt/CeO_2 based catalysts [5]. This outcome has been confirmed also by other recent studies [10,12].

Furthermore, Pt on CeO_2 is intrinsically a system with a highly dynamic nature. The state of platinum is dependent on its treatment history and can be changed thoroughly at temperatures even below 300 °C [5]. Hence, structure–activity correlations should be derived not only by pre- and postmortem analysis of the catalyst state but especially by tracking the evolution of the single sites under reaction conditions, i.e., *in situ/operando*. So far, the majority of *in situ/operando* studies on Pt SACs have focused on weakly interacting supports, i.e., Al_2O_3. For example, Dessal et al. [13] used a combination of *operando* X-ray absorption near edge structure (XANES) spectroscopy and diffuse reflectance infrared Fourier transform spectroscopy (DRIFTS) to monitor the evolution of Pt single sites on alumina during CO oxidation. Their results suggest partial clustering of Pt atoms, more pronounced during the first light-out, which leads to an increased CO oxidation activity in further cycles. In contrast, by using density functional theory (DFT) and molecular dynamics, López et al. have recently evidenced that Pt single sites undergo a dynamic charge transfer on CeO_2 (100) surface and the presence of short-lived Pt^+ species coordinated to two O atoms might play a major role in regulating the catalytic activity [1]. On a multifaceted commercial CeO_2, the reversible formation of small Pt clusters as active species during CO oxidation light-off was recently reported by our group. By means of advanced spectroscopic studies and DFT calculations, Maurer et al. [14] uncovered that Pt single sites are necessarily slightly reduced and agglomerate in small clusters before the CO oxidation onsets.

As a next step, the present study focuses on elucidating the behavior of the Pt/CeO_2 single site catalyst under more complex reaction conditions, including CO/C_3H_6 oxidation in the presence and absence of water. In order to identify further mechanistic aspects, we supplemented the activity data with in-depth characterization and more systematic analysis of the *operando* spectroscopic results collected during activity onset and light-off. A special focus was placed on the low temperature region, which allowed us to better understand the origin of the poor activity during oxidation reactions for Pt single site catalysts. More specifically, a multivariate curve resolution-alternating least square (MCR-ALS) algorithm [15,16] was applied to the high-energy resolution-fluorescence-detected XANES (HERFD-XANES) data obtained during exposure of the Pt/CeO_2 catalysts to various model and reaction conditions. This approach, increasingly applied in heterogeneous catalysis [15,17–20], enables us to derive minute spectral features, i.e. caused by the adsorption of different gas phase species, and is therefore ideal to identify noble metal state, abundance and evolution.

2. Results and Discussion

2.1. Basic Characterization

In line with our previous investigations [14], no Pt nanoparticles could be identified in the TEM micrographs (Figure 1) obtained for the Pt/CeO_2 catalyst (0.94 wt.% noble metal loading found by inductively coupled plasma-optical emission spectroscopy, ICP-OES, analysis) upon the hydrothermal treatment in 10% O_2, 10% H_2O/N_2 at 800 °C for 16 h. The formation of highly or atomically dispersed Pt species is indicated also by the XRD data (Figure 1), as apart from ceria no characteristic reflections for Pt and PtO_x can be observed. After the hydrothermal treatment, the crystallite size (evaluated via Scherrer equation) of the ceria support is about 30 nm. The sample exhibits a specific surface area of 30 m^2/g.

A further confirmation of the high dispersion of Pt species is given by the presence of two Raman bands (Figure S1) at 552 and 667 cm^{-1}, previously associated with Pt–O–Ce and Pt–O vibrations and typical for platinum single sites [11]. X-ray photoelectron spectroscopy (XPS) measurements highlight a primary +2 oxidation state for Pt species (84 at. %). A minor fraction (16 at. %) is present as Pt^{4+} species, in quantity comparable with previous findings [11]. The atomic Pt:Ce ratio, determined by quantitative surface analysis, is 2.5:97.5. Finally, the Fourier transforms of the extended X-ray absorption fine structure (EXAFS) data collected for the hydrothermally treated Pt/CeO_2 catalyst shows two main pronounced backscattering contributions (Figure S2). The first one, at about 2.01 Å, can

be assigned to the Pt–O interaction. The second feature at 3.13 Å is slightly shifted with respect to the Pt-Pt distance, and has been previously assigned to a Pt–Ce distance [21], endorsing the intimate contact between the Pt ions and the support. Altogether, these results confirm that Pt species are indeed highly dispersed and located on the surface of the support.

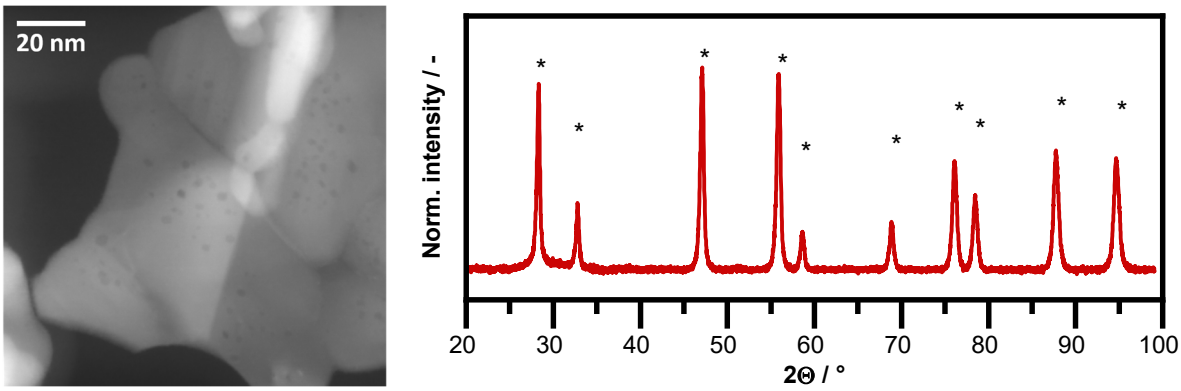

Figure 1. TEM micrograph of Pt-single site samples evidence the absence of Pt nanoparticles (left); XRD diffractogram of the sample (right). Stars indicate the reflections typical for CeO_2.

2.2. Catalytic Activity

The catalytic activity of Pt single sites on CeO_2 under lean (oxygen-rich) conditions was investigated for CO, C_3H_6, and CO/ C_3H_6 oxidation under dry conditions and for CO/ C_3H_6 oxidation also under wet conditions. The temperature values for 50% (T_{50}) and 90% conversion (T_{90}) are reported in Figure 2 (for conversion curves, see Figures S3–S5). In line with recent studies [4,5,11], the CO oxidation activity (1000 ppm CO, 8% O_2 in N_2) is only modest at low temperatures, with a T_{50} = 194 °C and T_{90} = 203 °C. The conversion is significantly inferior to that obtained for the corresponding Pt/CeO_2 catalysts after reduction and formation of Pt nanoparticles, i.e., T_{50} = 69 °C [14]. For the Pt single site catalyst, the light-out conversion is shifted towards lower temperature (T_{50} = 175 °C), showing a normal hysteresis profile [22].

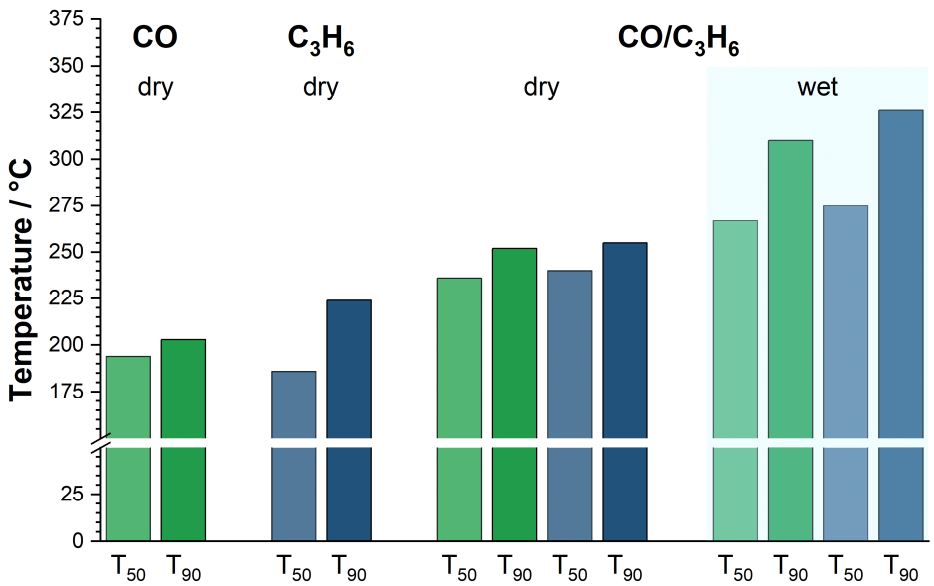

Figure 2. Temperatures of 50% (lighter shades) and 90% (darker shades) conversion for CO (green), C_3H_6 (blue) and CO/C_3H_6 oxidation reactions catalyzed by Pt single site.

The propene oxidation (150 ppm C_3H_6, 8% O_2 in N_2) displays a slightly lower onset temperature compared to CO conversion, and a T_{50} at 186°C. Nonetheless, full conversion is only reached above 300 °C. When both CO and C_3H_6 are present in the gas mixture, the ignition temperature for CO oxidation is delayed by 40 °C (T_{50} = 236 °C), while C_3H_6 oxidation is even more strongly affected (ΔT = 56 °C, T_{50} = 240 °C). This behavior is due to the competitive adsorption on the active sites of CO and C_3H_6 oxidation intermediates (different carboxylic, bicarbonate and formate species) [22]. During cooling down, the two curves again follow a very similar behavior, with extinction temperatures of T_{50} = 222 °C for CO and T_{50} = 227 °C for C_3H_6. In the presence of CO, the propene conversion profile shows a wide normal hysteresis loop, in line with what is commonly observed for combined mixtures with low C_3H_6:CO ratios [23]. In the presence of H_2O, a shift of the oxidation activity towards higher temperatures was observed, with a T_{50} at 267 °C for CO conversion and at 275 °C for C_3H_6 oxidation.

Previous studies reported a beneficial impact of water (in low amount) on the oxidation activity due to the formation of hydroxyl species [10]; therefore, further investigations will be needed to unravel in detail the consequence of wet conditions on the catalytic performances of single-site catalysts.

2.3. In Situ/Operando Characterization

To fully understand the structural variations and their impact on the catalytic behavior, it is of outmost importance to investigate in detail the interaction of the Pt single sites with the gas phase. We focused on CO oxidation as a model reaction. For this purpose, we resorted to HERFD-XANES, which combines the element specificity detection of standard X-ray absorption spectroscopy (XAS) with an improved spectral resolution, necessary to emphasize even faint modifications in the spectral features [24]. Thanks to a resolution better than the core-hole lifetime broadening that limits conventional XAS, with HERFD-XANES it is possible to reveal small variations in intensity and position that would not be visible with standard XANES. During catalyst exposure to different reaction conditions, the fluorescence selected with three spherically bent (R = 1 m) Ge (660) analyzer crystals (in Rowland geometry) at the maximum of the Pt-$L_{\alpha 1}$ emission line (9442 eV) was recorded with an avalanche photodiode detector, while the incident energy was scanned around the Pt-L_{III} absorption edge (11564 eV). The *operando* setup, including the capillary reactor, gas dosage and analytics, is depicted in Figure 3. The microreactor is highly versatile and perfectly mimics a conventional plug-flow reactor, allowing us to collect catalytic activity (via Fourier-transform infrared spectrometer and mass spectrometer) at the same time as structural data [25].

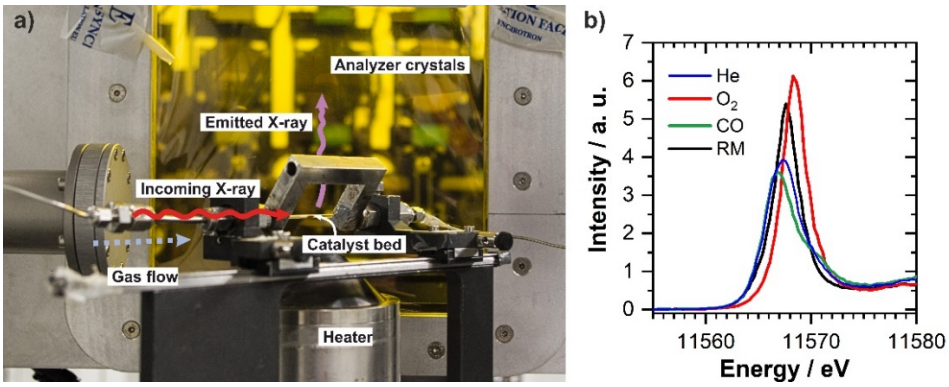

Figure 3. (**a**) Schematics of the *operando* HERFD-XAS setup at BM16 (ESRF, Grenoble). (**b**) *In situ* Pt L_{III}-edge HERFD-XANES spectra recorded at room temperature in different gas atmospheres: 10% O_2/He (red), He after temperature programmed oxidation (blue), 1000 ppm CO/He (green) and reaction mixture (RM, 1000 ppm CO, 10% O_2 in He, black).

Three model gas mixtures were used to derive spectral features of Pt interaction with reactant molecules: inert atmosphere, 10% O_2 in He and 1000 ppm CO in He. The corresponding HERFD-XANES spectra obtained at room temperature are shown in Figure 3 together with that collected in the reaction mixture. In helium, the white line peaks at 11567.3 eV and has a moderate intensity, suggesting an oxidation state of +2 (for a comparison with reference Pt^{2+} compounds, see Figure S6). When the sample is exposed to 10% O_2 there is a strong increase in overall intensity and a shift of the maximum towards higher energies (11568.3 eV, ΔE = +1.0 eV), attesting a further oxidation of the Pt single sites due to the interaction with molecular oxygen. On the contrary, if the sample is subjected to CO, a partial reduction occurs [24]. This can be evinced from the shift of the maximum towards lower energies (11566.8 eV, ΔE = −0.5 eV) and a slight decrease in white line intensity. In addition, a shoulder at 11567.1 eV is additionally present. The reduction is only partial, with the probable formation of $Pt^{\delta+}$ species. For metallic Pt^0 nanoparticles, the maximum is further shifted toward lower energy (11565.8 eV) and intensity (Figure S6).

Under CO oxidation reaction mixture (1000 ppm CO, 10% O_2 in He), the presence of oxygen prevails at room temperature and induces an increase in white line intensity in comparison to the noble metal state in 1000 ppm CO/He (cf. Figure 3b). However, in this case the white line shifts with respect to the sample in 10 % O_2/He, indicating the adsorption of CO on the noble metal surface. Overall, the fact that HERFD-XANES reveals such a strong response due to changes in the gas phase further confirms the location of most Pt single sites on ceria surface.

To track the dynamic behavior of the Pt single sites, HERFD-XANES data were collected *in situ/operando* in the different reaction mixtures between 50 to 400 °C (in a stepwise fashion, every 50 °C), (Figure 4a–d). The increase of temperature led to pronounced changes of the white line region, even for the catalyst exposed to 10% O_2/He. Above 50 °C, the main peak starts losing intensity and shifts towards lower energy; at 150 °C, there is a clear difference, with the overall intensity reduced to about 2/3 of the starting one and the maximum now positioned at 11567.1 eV (showing a shift with respect of the room temperature spectrum $\Delta E_{RT} = -1.2$ eV). This behavior points out that a stronger oxidation of Pt single sites occurs by adsorption of molecular oxygen at room temperature, which is later removed at temperatures above 100 °C. As the temperature further increases the changes become subtler, with only minor variations in the main white line region, while a shoulder at 11570.6 eV becomes more evident.

Additionally, under reducing conditions, in 1000 ppm CO/He, no changes are detected at 50 °C. At higher temperatures, on the other hand, the HERFD-XANES white line gradually loses intensity and becomes broader. Up to 150 °C, changes mainly interest the intensity, while the white line position shows only a minor increase ($\Delta E_{RT} = +0.3$ eV). From 200 °C on, conversely, the intensity is almost constant while the maximum shifts toward lower energies ($\Delta E_{RT} = -1.2$ eV). This could be interpreted as follows: at low temperatures CO gradually adsorbs on Pt^{2+} sites, but starting around 100 °C the presence of CO leads to a change in the noble metal structure. In line with previous DFT calculations [14], partial reduction of the single sites (hence the reduction of intensity) occurs initially, leading to the formation of isolated $Pt^{\delta+}$ species coordinated to CO ($Pt^{\delta+}$-CO). Above 150 °C, on the other hand, the variations in the spectral features likely indicate the development of Pt clusters, since the final spectrum is similar to the reference sample containing Pt nanoparticles (Figure S6).

Operando HERFD-XANES experiments under reaction conditions (1000 ppm CO, 10% O_2 in He) revealed a much more complex behavior. Analogously to the changes observed in 10% O_2/He, up to 100 °C the white line decreases in intensity while maintaining the position. In the temperature interval 100–150 °C, a further decrease in intensity is accompanied also by a shift in maximum position ($\Delta E_{RT} = -0.8$ eV), with the appearance of a slight shoulder at 11570.6 eV. The temperature of 150 °C also corresponds to the onset of CO oxidation. Simultaneously with the increase of CO conversion, a further slight shift in the white line position occurs ($\Delta E_{RT} = -1.0$ eV), while at the same time the shoulder at

11570.6 eV becomes more evident. Above 250 °C (full conversion), the spectrum resembles the one collected at the same temperature in 10% O_2, which is due to the CO consumption mainly at the inlet of the catalyst bed [26]. Nonetheless, throughout the whole experiment, the white line intensity is lower under reaction conditions.

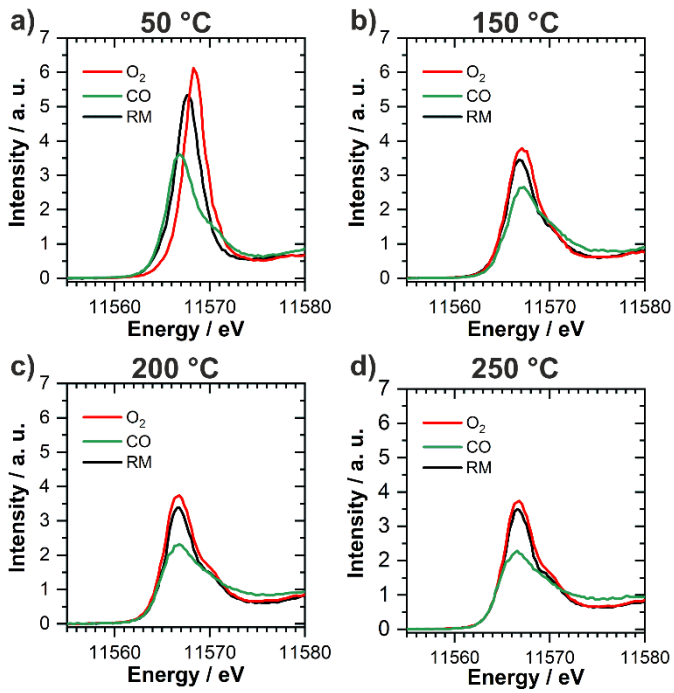

Figure 4. (**a**–**d**) Evolution with temperature of HERFD-XANES spectra of Pt singles sites on CeO_2 under different gas atmospheres, as collected at the middle position of the catalyst bed (red curves: 10% O_2/He, green curves: 1000 ppm CO/He and black curves: reaction mixture with 1000 ppm CO, 10% O_2 in He).

The multiple variations in Pt structure observed during CO oxidation were assigned based on a multivariate curve resolution-alternating least squares (MCR-ALS) algorithm [27–29], which was employed to decompose the experimental data, isolate spectra corresponding to individual species and evaluate their concentration. This approach was applied considering both the *operando* data as well as the spectra acquired during temperature programmed oxidation (TPO, 10% O_2/He) and reduction (TPR, 1000 ppm CO/He). Principal component analysis performed prior to the MCR-ALS investigation estimated a total of five pure species concurring in the changes visible under reaction conditions. This outcome reveals an additional species for the low temperature region in comparison to the results reported by Maurer et al. [14].

Based on the variations observed in the Pt HERFD-XANES profile as a function of temperature and model gas mixtures, the obtained MCR-ALS spectra (Figure 5) were tentatively assigned to the following states:

(i) Pt^{4+}-"O_2" or peroxo species [14,30] that might form by adsorption of molecular O_2 at low temperatures onto CeO_2 surface [31]. These species are expected to have a poor stability and release the absorbed oxygen already at room temperature if the gas atmosphere changes (Figure 3).

(ii) Pt^{4+}-"O" highly oxidized single sites located at four-fold hollow sites on the ceria surface by Pt–O–Ce bonds and involving strongly bound oxygen atoms; this species is predominant at low temperatures in the as prepared catalyst in inert atmosphere.

(iii) Pt^{2+} located at four-fold hollow sites present or generated at the {211}/{221} edges or on the {110} facet of ceria support [14]; due to the high thermodynamic stability, this species emerges during single-site catalyst preparation at high temperature; under

reaction conditions, bare Pt^{2+} forms during heating up to 200 °C upon desorption of oxygen from Pt^{4+}-"O", a process apparently not influenced by the CO presence (Figure S8); finally, this species appears at higher temperatures once CO oxidation front shifts towards the inlet of the catalyst bed.

(iv) $Pt^{\delta+}$-CO forms by partial reduction of bare Pt^{2+} single sites; the appearance of this intermediate state is indicated by the slight decrease of the white line intensity, which is in line with the variation of the HERFD-XANES spectra profile during Pt/CeO_2 reduction in 1000 ppm CO/He (Figure 4) as the temperature increases.

(v) $Pt_x^{\Delta+}$-CO clusters, generated by nearby migration of the single atoms above 125 °C and emerging simultaneously with the CO oxidation onset.

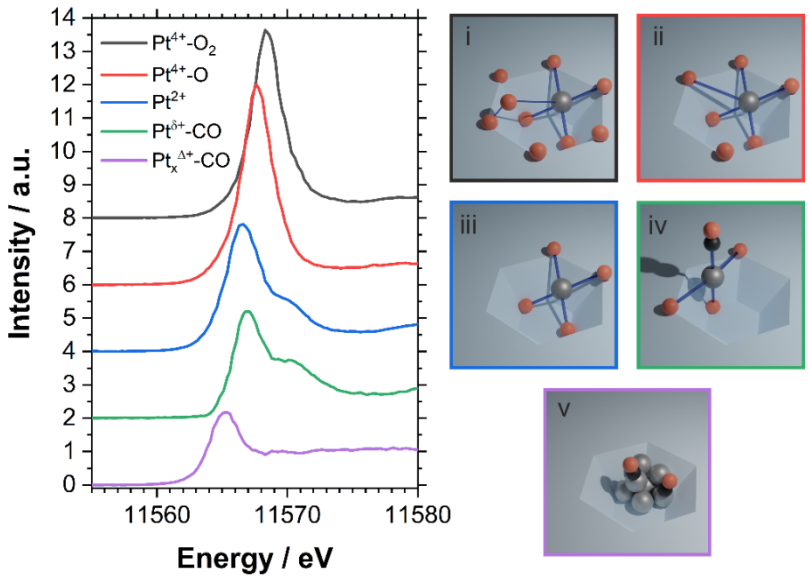

Figure 5. Reference HERFD-XANES spectra of pure Pt species present during CO conversion as determined via MCR-ALS (left) and corresponding schematic representation of the structure of the identified species (right; grey metallic spheres represent Pt atoms, red: O and black C). See text for detailed description of structures (**i**)–(**v**) shown on the right.

The concentration profiles (Figure 6) extracted by the MCR-ALS routine (see Figure S9 for examples of spectra fitted with the MCR-ALS derived references) during CO oxidation show that at low temperature the second Pt^{4+}-"O" species is predominantly present under reaction conditions. At 50°C, Pt^{4+}-"O_2" and Pt^{2+} concur only with about 10 at. % each. As the temperature increases, oxygen is readily desorbed, as the rapidly decaying profile of the Pt^{4+}-"O" oxidized species confirms. At 125 °C the majority of the noble metal single sites (ca. 50 %) are present as bare Pt^{2+} species and about 20 at. % of all Pt has already restructured as $Pt^{\delta+}$-CO. However, the partial reduction of the single sites does not seem to affect the catalyst activity (dotted curve in Figure 6). For Pt/CeO_2 catalysts, a Mars-van Krevelen mechanism is generally assumed at low temperature [2,32,33], involving chemisorbed CO and lattice oxygen at the ceria-noble metal interface. Previous studies have shown that CO adsorbes in an atop geometry at low coverages, switches to a bridge configuration if the CO surface concentration increases and returns to the atop state for close to monolayer coverage [34,35]. The adsorption at both the atop and bridge sites is additionally affected by the Pt surface charge, a factor highly relevant for single site catalysts due to their strong interaction with the support. As shown by Gunasooriya and Sayes [36], at low CO coverage an increase of the Pt charge swithches the CO adsorption preference towards a bridge geometry since the Pt–C bond streches to a greater extent at the atop site due to a more directional interaction between the Pt d_z^2 states and the CO 5σ molecular orbital. Under identical reaction conditions, the adsorption of CO was suggested to adsorb in the atop geometry on Pt nanoparticles supported on alumina but

in bridged configuration if the noble metal particles are deposited on CeO_2 [32]. The prominent effect of ceria on the CO adsorption sites has also been demonstrated for differently treated Pt/CeO_2-based catalysts by *in situ* diffuse reflectance infrared Fourier transform spectroscopy investigations [37,38], with pronounced effects on the oxidation activity. Despite the fact that CO coverage varies along the catalyst bed during the light-off, the adsorption of CO on the $Pt^{\delta+}$ single sites probably occurs in an atop geometry for the Pt/CeO_2 catalyst used in this study, as also indicated by the shape of the HERFD-XANES spectra [32]. This is mainly due to the submonolayer coverage of the noble metal on the ceria support. Hence, the adsorption should not be significantly affected by CO-CO interactions but only by the interplay with ceria.

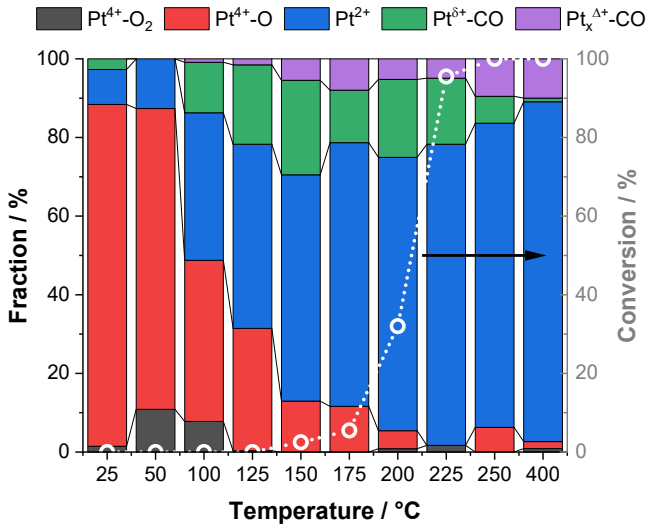

Figure 6. Fraction of the different Pt species at the middle of the catalyst bed, as determined by MCR-ALS and conversion of CO (empty circles connected via dotted line) as function of temperature in reaction mixture (1000 ppm CO, 10% O_2 in He).

Although the CO is adsorbed on the platinum sites, it seems that below 125 °C the interfacial lattice oxygen cannot play an active role in the oxidation reaction due to the strong binding energy in Pt–O–Ce. According to the DFT calculations reported by Maurer et al. [14], the bond between Pt and ceria can only be broken above 150 °C and subsequently the mobility of oxygen increases. A further consequence is that the mobility of Pt species also improves, which is indicated by the appearance of a new $Pt_x^{\Delta+}$ cluster species in the *operando* HERFD-XANES data. This process is probably also promoted by the slight increase of temperature due to the reduction of Pt^{2+} to Pt by CO, and simultaneous reduction of the interface ceria. The formation of noble metal clusters during CO oxidation has been speculated also by Dessal et al. for Pt on Al_2O_3, in a similar temperature range (150–200 °C) [13], but their presence was evident only after cooling down to room temperature. The formation of these species has a significant impact on the oxidation reaction as an outbreak in CO conversion is observed immediately despite their low concentration. In fact, the overall fraction of $Pt_x^{\Delta+}$ does not grow over 10 at. %. On the one hand, due to their high dispersion and atomic exposure, an apparently small fraction of $Pt_x^{\Delta+}$ clusters is probably sufficient to ensure a high CO conversion. On the other hand, this is due to a higher CO conversion at the inlet of the catalyst bed as the temperature increases [26], which leads to the exposure of the mid and end regions mostly to a O_2/He gas mixture. A higher $Pt_x^{\Delta+}$ concentration is therefore expected for the inlet section of the catalyst bed, whereas the small clusters downstream in the catalyst bed are redispersed. Due to the hysteresis profile of the CO conversion (Figure S3), the reformation of the $Pt_x^{\Delta+}$ clusters is not favored during cooling, as the temperature is probably too low for single site migration when the CO concentration reaches again higher values along the catalyst bed. The role of $Pt_x^{\Delta+}$ formation needs also to be evaluated during oxidation of other

species (e.g., C_3H_6), and the influence of water requires equal attention in future (see, e.g., influence of catalytic performance in Figure 1). For instance, preliminary HERFD-XANES data recorded during CO TPR in absence or presence of water (<6% H_2O in the gas feed) show that under wet conditions the intensity of the white line is slightly higher than that of the corresponding spectrum in dry atmosphere (Figure 7). This indicates that the oxidation state of Pt species is, at a given temperature, indeed higher in the presence of water and the formation of $Pt_x^{\Delta+}$ is hindered, leading to an onset of the catalytic activity at higher temperature. However, while this difference in oxidation state is small under the investigated conditions, the trend can already be unambiguously seen. Here, further experiments in the presence of oxygen and optionally propene, as well as higher amounts of water, could give a holistic picture on the effect of water.

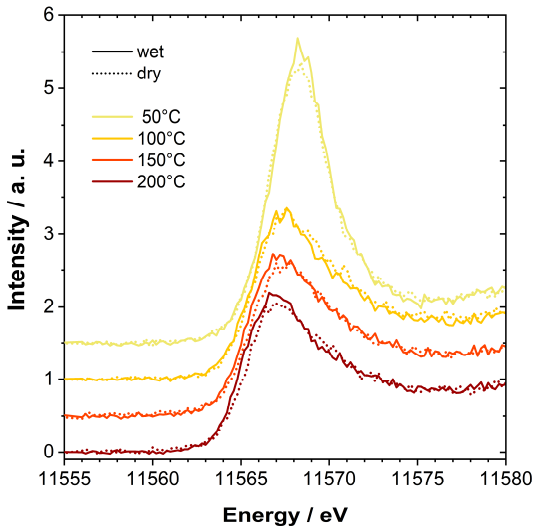

Figure 7. HERFD-XANES spectra recorded during CO temperature programmed reduction (1000 ppp Co/He), in absence (dotted lines) or presence (solid lines of water in the gas feed (H_2O < 6%).

3. Materials and Methods

Prior to synthesis, the commercial ceria support (MEL chemicals, Manchester, UK) was calcined at 700 °C for 5 h in static air. The catalysts were prepared via a robot-controlled incipient wetness impregnation (IWI) procedure, using an Accelerator SLT106 Parallel Synthesizer-SLT CATIMPREG (ChemSpeed Technologies, Füllinsdorf, Switzerland) [39]. The ceria support (1 g) was placed in a batch reactor, and 0.16 mL of tetraamine platinum nitrate (99,995%, Sigma Aldrich, Taufkirchen, Germany) solution (25.8×10^{-3} M) was added. This additional step was repeated until the desired platinum weight loading (1 wt%) was achieved. Between each addition, samples were dried under reduced pressure for 20 min at 70 °C. The final catalyst was further calcined at 500 °C for 5 h in static air. To finally generate the single sites, the sample was hydrothermally aged in 10% O_2 and 10% H_2O in N_2 at 800 °C for 16 h.

3.1. Catalytic Activity Tests

The CO oxidation activity of the Pt/CeO_2 catalysts was evaluated in a plug flow reactor (ID: 8.0 mm, OD: 10.0 mm) using a granulated catalyst powder and silica in physical mixture (mass ratio 1:9; total amount: 500 mg; sieve fraction: 125–250 µm). Two thermocouples were placed up- and downstream of the catalyst bed to monitor the temperature inside the reactor. The upstream one was also used to control the furnace. For the conversion tests, the catalyst was heated in an oxygen-rich atmosphere (1000 ppm CO/150 ppm C_3H_6, 6.6% H_2O and 8% O_2; weight hourly space velocity of 60,000 l g_{Pt}^{-1} h^{-1}) from 70 °C to 500 °C with 10 K/min and held at 500 °C for 1 h. Each light-off test was repeated two times.

3.2. Ex Situ Characterization

ICP-OES—The platinum loading in the final catalyst was determined by inductively coupled plasma optical emission spectrometry at the Institute for Applied Materials (IAM) of the Karlsruhe Institute of Technology (Karlsruhe, Germany). Prior to the analysis, the samples were digested using acids and high pressure.

BET—The specific surface area and total pore volume were determined by N_2 physisorption. The Brunauer–Emmett–Teller method to evaluate the experimental data. The samples were pretreated at 300 °C under reduced pressure (BELprep II, BEL Inc., Osaka, Japan). The N_2 physisorption was performed using a BELsorp II mini (BEL Inc., Osaka, Japan).

TEM—High angle annular dark-field imaging (HAADF) scanning transmission electron microscopy was performed at the laboratory for electron microscopy at the KIT (Karlsruhe, Germany) using a FEI Tecnai Osiris (Scanning) Transmission Electron Microscope (FEI Deutschland GmbH, Dreieich, Germany) at 80–300 kV.

XRD—Powder X-ray diffraction data were acquired using a Bruker D8 advance XRD (Bruker, Karlsruhe, Germany). The investigated 2Θ range was 20–100°, with a step size of 0.0162°. The mean crystallite size of ceria was estimated via the Scherrer equation (applied on reflexes at 28°, 33° and 47°, corresponding to reflections (111), (200) and (220) respectively), using a dimensionless shape factor of 0.94.

3.3. In Situ Characterization

A capillary micro reactor was used as *in situ* cell [40], using a hot air gas blower (FMB Oxford, Oxford, UK) as heating source. Gases were dosed by mass flow controllers (Bronkhorst, AK Ruurlo, The Netherlands). The gas concentration in the product flow was monitored on-line by a mass spectrometer (Omnistar, Pfeiffer Vacuum, Asslar, Germany) and a Fourier transformed infrared spectrometer (Multigas 2000, MKS, Munich, Germany). For the tests, the capillary reactor (1.5 mm outer diameter, 1.48 mm inner diameter) was loaded with 14 mg of the granulated (100–200 µm) Pt/CeO_2.

Conventional XAS (X-ray absorption spectroscopy) at Pt L_{III}-edge was collected at the P65 beamline at the Deutsches Elektronen-Synchrotron (DESY, Hamburg, Germany), in fluorescence mode (step scanning collection). For energy selection, a Si(111) crystal monochromator was used, with an energy resolution of 1.4×10^{-4}. A silicon drift detector was used to detect and select the emitted radiation. The beam size was 0.2 mm × 1.4 mm (V × H). For transient measurements, X-ray absorption near edge spectra were collected from 11.413 to 11.905 keV, resulting in a time resolution of 6.1 min per scan or one spectrum every 19 K. Extended X-ray absorption fine structure (EXAFS) spectra were recorded at room temperature and in step-scanning mode. The acquisition range was set to 11.413 to 12.560 keV. An average of at least 2 spectra was taken, to improve signal quality.

High-Energy Resolved Fluorescence Detected X-ray Absorption Near Edge Structure (HERFD-XANES) measurements were recorded at the BM16/FAME-UHD beamline at the ESRF (Grenoble, France), in a Rowland configuration. A cryogenically cooled Si(220) double crystal monochromator was used to pitch the incident energy (Pt L_{III}-edge) on the sample, and three spherically bent Ge(660) crystals (R = 1 m) were used to select the energy of the emitted fluorescence radiation (Pt $L_{\alpha 1}$ emission line, 9442 eV). The beam size was set to 150 µm × 300 µm. Spectra were recorded in step scanning mode with an energy resolution of 1–2 eV. Further HERFD-XANES experiments to assess the impact of water were recorded at the P64 beamline at DESY (Hamburg, Germany), in a von Hamos configuration. In this case, a Si(311) double crystal monochromator was used for energy selection, while six Si(800) crystals were operated to select the energy of the emitted fluorescence radiation (Pt $L_{\alpha 1}$ emission line, 9443 eV).The temperature-resolved normalized HERFD-XAS dataset was analysed by using the chemometrics plugin available in the Fastosh software (version 0.10.3b, SOLEIL Synchrotron, Gif-sur-Yvette, France, 2021) [41]. This feature incorporates the multivariate curve resolution with alternating least squares analysis toolbox developed by Tauler et al. [28]. Prior to MCR-ALS fitting, the number of concurring species was

estimated by single value decomposition of the dataset. The derived structural states were further used for linear combination fitting of the *operando* HERFD-XANES data collected under various reaction conditions.

4. Conclusions

The results obtained in our study confirm the poor activity of the Pt/CeO_2 single site catalyst during CO and C_3H_6 oxidation. A low oxidation performance was obtained also for a gas mixture containing both CO and C_3H_6 gases. In the presence of water, as encountered in real emission control application, the CO/C_3H_6 oxidation is even more limited. The systematic *operando* HERFD-XANES study conducted to understand the variation of Pt state during exposure to different reaction conditions uncovered a pronounced response of the Pt local structure to temperature and gas atmosphere changes. Pt L_{III}-edge HERFD-XANES data demonstrated that already at room temperature Pt single sites are undergoing a change in the electronic structure as a function of the ceria surface saturation with oxygen. The study also evinces a spontaneous reduction of Pt^{4+} to Pt^{2+} by release of molecular oxygen during heating the catalyst bed in an oxygen rich atmosphere, a process apparently not significantly influenced by the CO presence. MCR-ALS proved to be a very powerful method to extract chemically meaningful data from a multicomponent XANES dataset. Under reaction condition, five different states were identified for the noble metal single sites, including the reduction from Pt^{4+} to Pt^{2+} (below 125 °C) and finally to mobile $Pt^{\delta+}$ species, which form small $Pt_x^{\Delta+}$ clusters. Only after the appearance of these $Pt_x^{\Delta+}$ clusters, the onset of CO oxidation was observed. Our results clearly illustrate the dynamic nature of noble metal-based catalysts even if highly stabilized species such as Pt single sites are the principal players of the catalytic reaction. Their behavior should be studied also under more complex reaction conditions, i.e., in the presence of water, as present during real applications, and preferentially with advanced *operando* spectroscopic methods.

Supplementary Materials: The following are available online at https://www.mdpi.com/article/10.3390/catal11050617/s1, Figure S1: Raman spectra, Figure S2: CO conversion curves, Figure S3: C_3H_6 conversion curves, Figure S4: CO/C_3H_6 conversion curves, Figure S5: Pt L_{III} edge HERFD-XANES spectra of reference compounds, Figure S6: Pt species identified during TPO, Figure S7: Pt species identified during CO-TPR.

Author Contributions: Conceptualization, M.C. and J.-D.G.; formal analysis, P.D.; investigation, P.D. and F.M.; writing—original draft preparation, P.D. and F.M.; writing—review and editing, P.D., F.M., M.C. and J.-D.G.; visualization, P.D. and F.M.; supervision, M.C. and J.-D.G.; project administration, M.C.; funding acquisition, J.-D.G. All authors have read and agreed to the published version of the manuscript.

Funding: The authors thank the Deutsche Forschungsgemeinschaft (DFG, German Research Foundation) for financial support via SFB 1441-Project-ID 426888090, Project B3, as well as DESY (Hamburg, D) and ESRF (Grenoble, F) for beamtime at beamlines P65 and BM16, respectively. We acknowledge support by the KIT-Publication Fund of the Karlsruhe Institute of Technology.

Data Availability Statement: All data can be obtained from the corresponding author upon reasonable request.

Acknowledgments: The authors thank J. Wang and Y. Wang (IFG, KIT) for XPS analysis. A. Gänzler, D. Zengel, P. Lott, G. Nails and V. Marchuk (ITCP, KIT) and D. Doronkin (IKFT, ITCP) are gratefully acknowledged for assistance during *operando* XAS and HERFD-XANES experiments. Furthermore, we thank A. Deutsch and J. Pesek (ITCP, KIT) for technical support with respect to catalyst preparation, characterization and testing as well as H. Störmer (LEM, KIT) and T. Bergfeldt (IAM-AWP, KIT) for HAADF-STEM and ICP-OES analysis, respectively. Finally, M. Rovezzi, A. Aguilar (BM16, ESRF), E. Welter, R. Nemausat, M. Herrmann (P65, DESY) and A. Kalinko (P64, DESY) are thanked for the support during beamtime at the corresponding beamlines.

Conflicts of Interest: The authors declare no conflict of interest.

References

1. Daelman, N.; Capdevila-Cortada, M.; López, N. Dynamic charge and oxidation state of Pt/CeO_2 single-atom catalysts. *Nat. Mater.* **2019**, *18*, 1215–1221. [CrossRef] [PubMed]
2. Beniya, A.; Higashi, S. Towards dense single-atom catalysts for future automotive applications. *Nat. Catal.* **2019**, *2*, 590–602. [CrossRef]
3. Nagai, Y.; Hirabayashi, T.; Dohmae, K.; Takagi, N.; Minami, T.; Shinjoh, H.; Matsumoto, S. Sintering inhibition mechanism of platinum supported on ceria-based oxide and Pt-oxide–support interaction. *J. Catal.* **2006**, *242*, 103–109. [CrossRef]
4. Jones, J.; Xiong, H.; DeLaRiva, A.T.; Peterson, E.J.; Pham, H.; Challa, S.R.; Qi, G.; Oh, S.; Wiebenga, M.H.; Hernández, X.I.P.; et al. Thermally stable single-atom platinum-on-ceria catalysts via atom trapping. *Science* **2016**, *353*, 150–154. [CrossRef]
5. Gänzler, A.M.; Casapu, M.; Vernoux, P.; Loridant, S.; Aires, F.J.C.S.; Epicier, T.; Betz, B.; Hoyer, R.; Grunwaldt, J. Tuning the Structure of Platinum Particles on Ceria In Situ for Enhancing the Catalytic Performance of Exhaust Gas Catalysts. *Angew. Chem. Int. Ed.* **2017**, *56*, 13078–13082. [CrossRef] [PubMed]
6. Golunski, S.E.; Hatcher, H.A.; Rajaram, R.R.; Truex, T.J. Origins of low-temperature three-way activity in Pt/CeO_2. *Appl. Catal. B Environ.* **1995**, *5*, 367–376. [CrossRef]
7. Moses-DeBusk, M.; Yoon, M.; Allard, L.F.; Mullins, D.R.; Wu, Z.; Yang, X.; Veith, G.; Stocks, G.M.; Narula, C.K. CO Oxidation on Supported Single Pt Atoms: Experimental and ab Initio Density Functional Studies of CO Interaction with Pt Atom on θ-Al_2O_3(010) Surface. *J. Am. Chem. Soc.* **2013**, *135*, 12634–12645. [CrossRef]
8. Lu, Y.; Zhang, Z.; Lin, F.; Wang, H.; Wang, Y. Single-atom Automobile Exhaust Catalysts. *ChemNanoMat* **2020**, *6*, 1659–1682. [CrossRef]
9. Bera, P.; Priolkar, K.R.; Gayen, A.; Sarode, P.R.; Hegde, M.S.; Emura, S.; Kumashiro, R.; Jayaram, V.; Subbanna, G.N. Ionic Dispersion of Pt over CeO_2 by the Combustion Method: Structural Investigation by XRD, TEM, XPS, and EXAFS. *Chem. Mater.* **2003**, *15*, 2049–2060. [CrossRef]
10. Nie, L.; Mei, D.; Xiong, H.; Peng, B.; Ren, Z.; Hernandez, X.I.P.; DeLaRiva, A.; Wang, M.; Engelhard, M.H.; Kovarik, L.; et al. Activation of surface lattice oxygen in single-atom Pt/CeO_2 for low-temperature CO oxidation. *Science* **2017**, *358*, 1419–1423. [CrossRef]
11. Pereira-Hernández, X.I.; DeLaRiva, A.; Muravev, V.; Kunwar, D.; Xiong, H.; Sudduth, B.; Engelhard, M.; Kovarik, L.; Hensen, E.J.M.; Wang, Y.; et al. Tuning Pt-CeO_2 interactions by high-temperature vapor-phase synthesis for improved reducibility of lattice oxygen. *Nat. Commun.* **2019**, *10*, 1–10. [CrossRef]
12. Datye, A.K.; Guo, H. Single atom catalysis poised to transition from an academic curiosity to an industrially relevant technology. *Nat. Commun.* **2021**, *12*, 1–3. [CrossRef] [PubMed]
13. Dessal, C.; Len, T.; Morfin, F.; Rousset, J.-L.; Aouine, M.; Afanasiev, P.; Piccolo, L. Dynamics of Single Pt Atoms on Alumina during CO Oxidation Monitored by Operando X-ray and Infrared Spectroscopies. *ACS Catal.* **2019**, *9*, 5752–5759. [CrossRef]
14. Maurer, F.; Jelic, J.; Wang, J.; Gänzler, A.; Dolcet, P.; Wöll, C.; Wang, Y.; Studt, F.; Casapu, M.; Grunwaldt, J.-D. Tracking the formation, fate and consequence for catalytic activity of Pt single sites on CeO_2. *Nat. Catal.* **2020**, *3*, 824–833. [CrossRef]
15. Cassinelli, W.H.; Martins, L.; Passos, A.R.; Pulcinelli, S.H.; Santilli, C.V.; Rochet, A.; Briois, V. Multivariate curve resolution analysis applied to time-resolved synchrotron X-ray Absorption Spectroscopy monitoring of the activation of copper alumina catalyst. *Catal. Today* **2014**, *229*, 114–122. [CrossRef]
16. Nunes, C.A.; Resende, E.C.; Guimarães, I.R.; Anastácio, A.S.; Guerreiro, M.C. In-situ Monitoring of the Structure of a Goethite-Based Catalyst during Methane Oxidation by X-Ray Absorption Near-Edge Structure (XANES) Spectroscopy Assisted by Chemometric Methods. *Appl. Spectrosc.* **2011**, *65*, 692–697. [CrossRef]
17. Rabeah, J.; Briois, V.; Adomeit, S.; La Fontaine, C.; Bentrup, U.; Brückner, A. Multivariate Analysis of Coupled Operando EPR/XANES/EXAFS/UV–Vis/ATR-IR Spectroscopy: A New Dimension for Mechanistic Studies of Catalytic Gas-Liquid Phase Reactions. *Chem. A Eur. J.* **2020**, *26*, 7395–7404. [CrossRef] [PubMed]
18. Bergman, S.L.; Dahlin, S.; Mesilov, V.V.; Xiao, Y.; Englund, J.; Xi, S.; Tang, C.; Skoglundh, M.; Pettersson, L.J.; Bernasek, S.L. In-situ studies of oxidation/reduction of copper in Cu-CHA SCR catalysts: Comparison of fresh and SO_2-poisoned catalysts. *Appl. Catal. B Environ.* **2020**, *269*, 118722. [CrossRef]
19. Fahami, A.R.; Günter, T.; Doronkin, D.E.; Casapu, M.; Zengel, D.; Vuong, T.H.; Simon, M.; Breher, F.; Kucherov, A.V.; Brückner, A.; et al. The dynamic nature of Cu sites in Cu-SSZ-13 and the origin of the seagull NOx conversion profile during NH_3-SCR. *React. Chem. Eng.* **2019**, *4*, 1000–1018. [CrossRef]
20. Kerkeni, B.; Berthout, D.; Berthomieu, D.; Doronkin, D.E.; Casapu, M.; Grunwaldt, J.-D.; Chizallet, C. Copper Coordination to Water and Ammonia in Cu^{II}-Exchanged SSZ-13: Atomistic Insights from DFT Calculations and in Situ XAS Experiments. *J. Phys. Chem. C* **2018**, *122*, 16741–16755. [CrossRef]
21. Gatla, S.; Aubert, D.; Flaud, V.; Grosjean, R.; Lunkenbein, T.; Mathon, O.; Pascarelli, S.; Kaper, H. Facile synthesis of high-surface area platinum-doped ceria for low temperature CO oxidation. *Catal. Today* **2019**, *333*, 105–112. [CrossRef]
22. Casapu, M.; Fischer, A.; Gänzler, A.M.; Popescu, R.; Crone, M.; Gerthsen, D.; Türk, M.; Grunwaldt, J.-D. Origin of the Normal and Inverse Hysteresis Behavior during CO Oxidation over Pt/Al_2O_3. *ACS Catal.* **2017**, *7*, 343–355. [CrossRef]
23. Abedi, A.; Hayes, R.; Votsmeier, M.; Epling, W.S. Inverse Hysteresis Phenomena During CO and C_3H_6 Oxidation over a Pt/Al_2O_3 Catalyst. *Catal. Lett.* **2012**, *142*, 930–935. [CrossRef]

24. Safonova, O.V.; Tromp, M.; Van Bokhoven, J.A.; De Groot, F.M.F.; Evans, J.; Glatzel, P. Identification of CO Adsorption Sites in Supported Pt Catalysts Using High-Energy-Resolution Fluorescence Detection X-ray Spectroscopy. *J. Phys. Chem. B* **2006**, *110*, 16162–16164. [CrossRef] [PubMed]
25. Grunwaldt, J.-D.; Clausen, B.S. Combining XRD and EXAFS with on-Line Catalytic Studies for in situ Characterization of Catalysts. *Top. Catal.* **2002**, *18*, 37–43. [CrossRef]
26. Gänzler, A.M.; Casapu, M.; Boubnov, A.; Müller, O.; Conrad, S.; Lichtenberg, H.; Frahm, R.; Grunwaldt, J.-D. Operando spatially and time-resolved X-ray absorption spectroscopy and infrared thermography during oscillatory CO oxidation. *J. Catal.* **2015**, *328*, 216–224. [CrossRef]
27. De Juan, A.; Jaumot, J.; Tauler, R. Multivariate Curve Resolution (MCR). Solving the mixture analysis problem. *Anal. Methods* **2014**, *6*, 4964–4976. [CrossRef]
28. Jaumot, J.; de Juan, A.; Tauler, R. MCR-ALS GUI 2.0: New features and applications. *Chemom. Intell. Lab. Syst.* **2015**, *140*, 1–12. [CrossRef]
29. Voronov, A.; Urakawa, A.; van Beek, W.; Tsakoumis, N.E.; Emerich, H.; Rønning, M. Multivariate curve resolution applied to in situ X-ray absorption spectroscopy data: An efficient tool for data processing and analysis. *Anal. Chim. Acta* **2014**, *840*, 20–27. [CrossRef] [PubMed]
30. Ferré, G.; Aouine, M.; Bosselet, F.; Burel, L.; Aires, F.J.C.S.; Geantet, C.; Ntais, S.; Maurer, F.; Casapu, M.; Grunwaldt, J.-D.; et al. Exploiting the dynamic properties of Pt on ceria for low-temperature CO oxidation. *Catal. Sci. Technol.* **2020**, *10*, 3904–3917. [CrossRef]
31. Huang, M.; Fabris, S. Role of surface peroxo and superoxo species in the low-temperature oxygen buffering of ceria: Density functional theory calculations. *Phys. Rev. B* **2007**, *75*, 081404. [CrossRef]
32. Gänzler, A.M.; Casapu, M.; Doronkin, D.E.; Maurer, F.; Lott, P.; Glatzel, P.; Votsmeier, M.; Deutschmann, O.; Grunwaldt, J.-D. Unravelling the Different Reaction Pathways for Low Temperature CO Oxidation on Pt/CeO_2 and Pt/Al_2O_3 by Spatially Resolved Structure–Activity Correlations. *J. Phys. Chem. Lett.* **2019**, *10*, 7698–7705. [CrossRef] [PubMed]
33. Kopelent, R.; Van Bokhoven, J.A.; Szlachetko, J.; Edebeli, J.; Paun, C.; Nachtegaal, M.; Safonova, O.V. Catalytically Active and Spectator Ce^{3+} in Ceria-Supported Metal Catalysts. *Angew. Chem.* **2015**, *127*, 8852–8855. [CrossRef]
34. Ertl, G.; Neumann, M.; Streit, K. Chemisorption of CO on the Pt(111) surface. *Surf. Sci.* **1977**, *64*, 393–410. [CrossRef]
35. Steininger, H.; Lehwald, S.; Ibach, H. On the adsorption of CO on Pt(111). *Surf. Sci.* **1982**, *123*, 264–282. [CrossRef]
36. Gunasooriya, G.T.K.K.; Saeys, M. CO Adsorption Site Preference on Platinum: Charge Is the Essence. *ACS Catal.* **2018**, *8*, 3770–3774. [CrossRef]
37. Gänzler, A.M.; Betz, B.; Baier-Stegmaier, S.; Belin, S.; Briois, V.; Votsmeier, M.; Casapu, M. Operando X-ray Absorption Spectroscopy Study During Conditioning of Pt-Based Catalysts and Its Implications for CO Oxidation. *J. Phys. Chem. C* **2020**, *124*, 20090–20100. [CrossRef]
38. Meunier, F.C.; Cardenas, L.; Kaper, H.; Šmíd, B.; Vorokhta, M.; Grosjean, R.; Aubert, D.; Dembélé, K.; Lunkenbein, T. Synergy between Metallic and Oxidized Pt Sites Unravelled during Room Temperature CO Oxidation on Pt/Ceria. *Angew. Chem. Int. Ed.* **2021**, *60*, 3799–3805. [CrossRef]
39. Kleist, W.; Grunwaldt, J.-D. *Modern Applications of High Throughput R&D in Heterogeneous Catalysis*; Hagemeyer, A., Volpe, A., Eds.; Bentham Science Publishers: Sharjah, United Arab Emirates, 2014; ISBN 9781608058723.
40. Grunwaldt, J.-D.; Baiker, A. In situ spectroscopic investigation of heterogeneous catalysts and reaction media at high pressure. *Phys. Chem. Chem. Phys.* **2005**, *7*, 3526–3539. [CrossRef]
41. Landrot, G. FASTOSH: A Software to Process XAFS Data for Geochemical & Environmental Applications. In Proceedings of the Goldschmidt Abstracts, Boston, MA, USA, 12–17 August 2018; p. 1402.